10

Discontinuity Detection from Inflection of Otsu's Threshold in Derivative of Scale-Space

Rahul Walia[1], David Suter[2] and Raymond A. Jarvis[1]
[1]*Monash University*
[2]*Adelaide University*
Australia

1. Introduction

Discontinuity detection is studied across disciplines of thermodynamics, chemistry, geology, manufacturing, equipment maintenance, signal processing, computer architecture (bit recognition), finance (jump processes to model markets) and image processing. In image processing an edge is often modeled as a discontinuity (Lindeberg, 1998). Hence discontinuity detection, can provide edge information for image analysis with applications in robotic vision, medical imaging, tomography and surveillance etc. Scale-Space theory (Koenderink, 1984; Lindeberg, 1994; Witkin, 1983), is a framework for multi-scale analysis of function/image. While there are non-Gaussian Scale-Space representations (Duits et al., 2003), this article is confined to widely accepted Gaussian Scale-Space (Babaud et al., 1986; Lindeberg, 1994). Existing Scale-Space literature is focused mainly on developing Scale-Space theory with a view to:

a. Study impact on underlying signals/images (Babaud et al., 1986; Koenderink, 1984; Lindeberg, 1998; Romeny, 1994; Witkin, 1983)
b. Determine appropriate scale(s) relevant to the image/signal(Lindeberg, 1994).
c. Extract information and knowledge to develop applications like feature detection, feature classification, image segmentation, image matching, motion estimation, shape computation and object recognition etc.
d. Correlate the Scale-Space framework with biological vision (Hubel & Wiesel, 1987; Koenderink & Doorn, 1992; Koenderink & van Doorn, 1987; Young, 1987).

Current Scale-Space literature, does not adequately explore the statistical component of Scale-Space. There are contextual applications of various statistical parameters (Rodriguez, 2006; Sakai & Imiya, 2009; Zagal et al., 2000), in contemporary Scale-Space research, but they are limited in scope to specific applications or/and statistics of image features like blob volume, clusters, thresholds etc. Researchers would be well-assisted if some theoretical basis were available for statistical assumptions in Scale-Space. In this article, we present a theoretical foundation for some statistical assumptions with regard to the derivative of a discontinuity in Scale-Space. A discontinuity has an infinitesimal existence in Scale-Space, which leads to the assumption of continuity of underlying image/function in any conventional Scale-Space analysis (Koenderink, 1984; Lindeberg, 1994). This article reveals that even though Scale-Space eliminates discontinuity at infinitesimal scale, the Probability

Density Function (PDF) of the derivative of a discontinuity retains its unbalanced bimodality in Scale-Space. This chapter makes following theoretical contributions:

1. Derivation of Probability Density Function (PDF) and Cumulative Distribution Function (CDF) for the derivative of a discontinuity in Scale-Space (Theorem 2).
2. Proof of bimodality (Theorem 3) and unbalance (Theorem 4) of the PDF of the derivative of a discontinuity in Scale-Space.
3. Proof that the Otsu's Threshold (OT) (Otsu, 1979) owing to its sensitivity to unbalanced and bimodal PDFs has different patterns in Scale-Space based on the presence / absence of a discontinuity:
   a. Transient Increase: Discontinuity present.
   b. Monotone Decrease: Discontinuity absent.

The above mentioned theoretical results, are then applied for a simultaneous solution of following problems in image processing (Figure 1):

1. Scale appropriate to the discontinuity.
2. Threshold appropriate to the discontinuity.
3. Boundaries of entities in images.

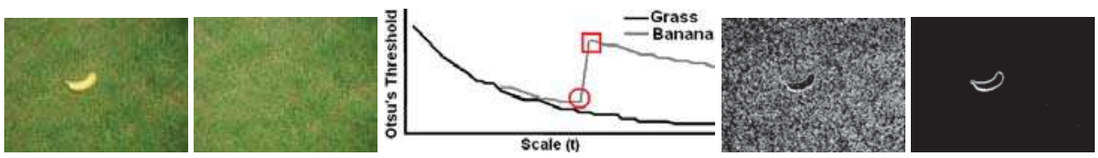

(a) (b) (c) (d) (e)

Fig. 1. OT Patterns in the absence and presence of a discontinuity (boundary). (a) **Banana**: Image with discontinuity (boundary).(b) **Grass**: Image without discontinuity (boundary). (c) OT Plots against Scale for "Grass" and "Banana". □ and ◯ : Upper and Lower points of inflection. (d), (e) Segmentation at lower and upper points of inflection respectively.

2. Statistical distributions of a Gaussian function

The term Gradient Magnitude in Scale-Space (GMSS) will be used hereon to represent

a. *In 1-D Non-Discrete Functions* The derivative of the Scale-Space representation of the functions
b. *In 2-D Discrete Images* The magnitude of the gradient (computed by Sobel operator) of Scale-Space representation of the images.

In this section, the statistical distributions of the GMSS of a discontinuity will be derived. The reason for doing so is to show that the PDF of the GMSS of a discontinuity is bimodal and unbalanced i.e. the probability of one mode far exceeds the probability of the other mode. A discontinuity is mathematically represented as a step function. Consequently the derivative of the discontinuity is a Dirac's Delta (Khuri, 2004) as shown in Figure 2. Convolution of the Dirac delta (δ)[1] with a Gaussian function will result in GMSS of a discontinuity.

[1] Since a Dirac's Delta is zero everywhere except at one point, therefore its PDF will be of the type shown in Figure 2. The PDF of a Dirac's Delta exists only at two points i.e. at ($x = 0$ and $x = \infty$) and is bimodal and unbalanced.

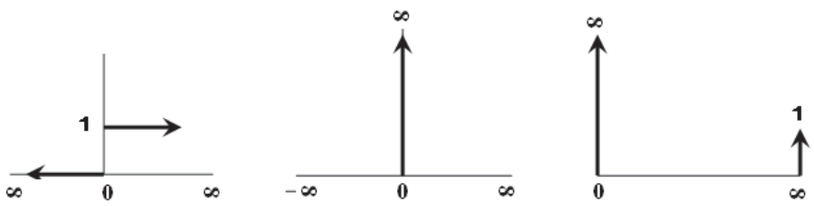

Fig. 2. Unit step function Dirac Delta PDF of Dirac Delta

Theorem 1. The GMSS $L'(x;t)$ of a Step function is given by a Gaussian Kernel G(x;t):

$$\begin{aligned} &L'(x;t) = G(x;t) \qquad where \\ &G(x;t) = \frac{e^{-\frac{x^2}{2t}}}{\sqrt{2\pi t}} : \text{Gaussian Kernel at Scale (t)} \\ &(-N < x < N : N \to \infty) : \text{Domain of the Function} \end{aligned} \tag{1}$$

Proof. For a Step function $H(x)$, the Scale-Space (SS) representation $L(x;t)$ is given by

$$H(x) = \left\{ \begin{matrix} 1 \; if \quad N > x > 0 \\ 0 \; if \; -N < x < 0 \end{matrix} \right\} \tag{2}$$

$$L(x;t) = H(x) \otimes G(x;t) \tag{3}$$

Convolution commutates with differentiation and the derivative of a Step function is a Dirac Delta ($\hat{\delta}(x)$) (Khuri, 2004) (Figure 2). Consequently:

$$\begin{aligned} &L'(x;t) = \frac{d}{dx}[H(x) \otimes G(x;t)] = \frac{d}{dx}[H(x)] \otimes G(x;t) = \hat{\delta}(x) \otimes G(x;t) \\ &where \qquad \hat{\delta}(x) = H'(x) = \left\{ \begin{matrix} \infty \; if \; x = 0 \\ 0 \quad if \; x \neq 0 \end{matrix} \right\} \end{aligned} \tag{4}$$

A Gaussian Kernel reduces to Dirac Delta at zero Scale i.e ($\hat{\delta}(x) = G(x;0)$), therefore (4) is equivalent to the convolution of two Gaussian Functions with scales ($t_1 = 0, t_2 = t$). Since $[G(x;t_1 + t_2) = G(x;t_1) \otimes G(x;t_2)]$ (Lindeberg, 1994), therefore (4) simplifies to:

$$L'(x;t) = G(x;t) \quad where \quad x \in 2N \qquad \square$$

Theorem 1 simplifies the GMSS of a discontinuity to a Gaussian Function, which in turn allows formulation of the statistical characteristics of the GMSS of a discontinuity.

2.1 PDF of a Gaussian function

Theorem 2. A continuous random variable **g** which takes the values $g \in (\frac{1}{\sqrt{2\pi t}}, \frac{1}{\sqrt{2\pi t}} e^{\frac{-N^2}{2t}} : N \to \infty)$, given by a Gaussian function $G(x;t)$ has following statistical distributions:

$$PDF: \qquad f_g(g) = \frac{t}{Ng\sqrt{-tlog_e(2\pi t g^2)}} \tag{5}$$

$$CDF: \qquad F_g(g) = \frac{\sqrt{-tlog_e(2\pi t g^2)}}{N} \tag{6}$$

Proof. Gaussian function ($G(x;t)$) is symmetric and provides a one to one, monotonic and inverse mapping between x and g, in each half of the Cartesian plane. Therefore a *uniformly distributed* random variable ($\mathbf{X}$) which takes the values $x \in (0, N : N \to \infty)$ in the positive spatial domain of the Gaussian function can derive the PDF and CDF for $\mathbf{g}$. The uniformly distributed PDF of ($\mathbf{X}$) is given by:

$$f_x(x) = \frac{1}{N} \text{ where } x \in \{0, N : N \to \infty\} \tag{7}$$

The equivalent PDF and the domain for the gaussian variable ($\mathbf{g}$) is given by:

$$f_g(g) \text{ where } g \in \left\{ \frac{1}{\sqrt{2\pi t}}, \frac{1}{\sqrt{2\pi t}} e^{\frac{-N^2}{2t}} : N \to \infty \right\} \tag{8}$$

The probabilities for both the random variables are equal in the mapped ranges :

$$\begin{aligned} &\int_{\frac{1}{\sqrt{2\pi t}}}^{g} f_g(g)\mathrm{d}g = \int_0^x f_x(x)\mathrm{d}x \quad where \\ &x = G^{-1}(g;t) = \sqrt{-t \log_e(2\pi t g^2)} \end{aligned} \tag{9}$$

Introducing a change of variable from x to g in the right hand side of (9) and solving:

$$\int_{\frac{1}{\sqrt{2\pi t}}}^{g} f_g(g)\mathrm{d}g = \int_{\frac{1}{\sqrt{2\pi t}}}^{g} f_x(x) \left\| \frac{d[G^{-1}(g;t)]}{dg} \right\| \mathrm{d}g \tag{10}$$

$$f_g(g) = \frac{t}{Ng\sqrt{-t log_e(2\pi t g^2)}} \tag{11}$$

The CDF [2] can be computed by integrating the PDF (11):

$$P[g \leq \mathbf{g} \leq \sqrt{2\pi t}] = F_g(g) = \frac{\sqrt{-t log_e(2\pi t g^2)}}{N} \qquad \square$$

Alternate proof of PDF($F_g(g)$), can be provided by replacing the value of (x) from (9) in the CDF ($F_x(x) = x/N$) of uniformly distributed variable $\mathbf{X}$ and then differentiating it w.r.t (g), which would provide expression (11).

2.2 Bimodality of the PDF of a Gaussian function

Theorem 3. The PDF $f_g(g)$ of a Gaussian function is bimodal.

Proof. The bimodality of the PDF can be proved by the existence of exactly one minima in the PDF ((Eisenberger, 1964; Kemperman, 1991; Schilling et al., 2002)). For a point (g_0) belonging to the domain of the PDF to be a minima, it's first derivative should be zero ($f_g^{'}(g_0) = 0$) and

[2] The correctness of the expression can easily be verified by replacing the term ($\sqrt{-t log_e(2\pi t g^2)}$) in CDF with x from (9). This gives ($P[0 \geq \mathbf{X} \geq x] = F_x(x) = x/N$) which is the expression of a CDF of a uniformly distributed variable ($\mathbf{X}$)

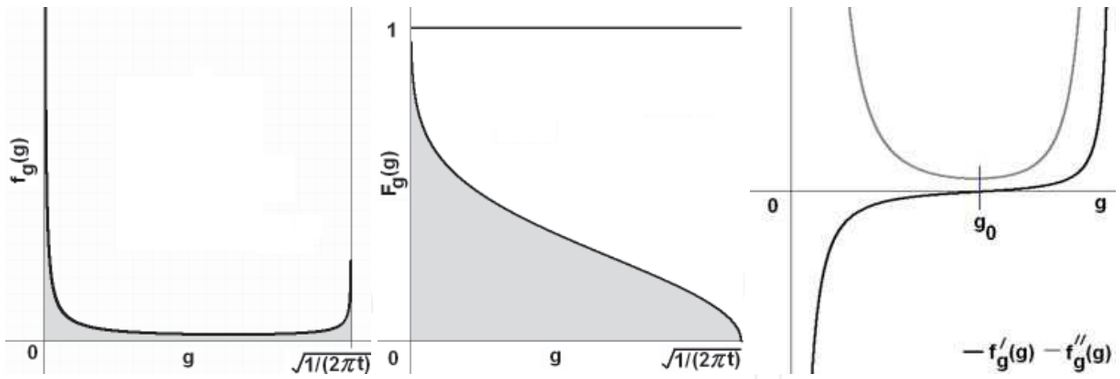

(a) PDF (b) CDF (c) Derivatives of the PDF

Fig. 3. PDF, CDF and derivatives (w.r.t. g) of the PDF of a Gaussian Function. The PDF has an inverse J-Shape. The derivatives show that only one minimum exists in the PDF making it bimodal.

it's second derivative should be positive ($f''_g(g_0) > 0$). The first and the second derivatives (with respect to g) of the PDF are given by:

$$f'_g(g) = \frac{t^2}{Ng^2(G^{-1}(g;t))^3} - \frac{t}{Ng^2G^{-1}(g;t)} \tag{12}$$

$$f''_g(g) = \frac{3t^3}{Ng^3(G^{-1}(g;t))^5} - \frac{3t^2}{Ng^3(G^{-1}(g;t))^3} + \frac{2t}{Ng^3(G^{-1}(g;t))} \tag{13}$$

The minima g_0 in the PDF can be located from the root(s) of (12)

$$\begin{aligned} \frac{t^2}{g_0^2(G^{-1}(g_0;t))^3} &= \frac{t}{g_0^2G^{-1}(g_0;t)} \\ \Rightarrow g_0 &= \frac{1}{\sqrt{2e\pi t}} \quad \forall \quad t > 0 \end{aligned} \tag{14}$$

Existence of only one root for the first derivative of the PDF, implies that only one extrema exists in the PDF. Substituting the value of g_0 from (14) into (13) and solving

$$f''_g(g_0) = 4\sqrt{2}t^2(e\pi)^{\frac{3}{2}} > 0 \tag{15}$$

From (14) and (15), g_0 is the (only) minima in the PDF, therefore it establishes the bimodality of the PDF (Figure 3). □

2.3 Unbalance in modes of the PDF of a Gaussian function

Theorem 4. The bimodal PDF $f_g(g)$ of the GMSS of a Step Discontinuity is unbalanced, i.e the probability of one mode is much greater than the other.

$$F_g(g_0) << 1 - F_g(g_0) \tag{16}$$

Proof. The probabilities of the two modes separated at g_0 can be computed from CDF (6)

$$\begin{aligned} P(g \geq g_0) &= F_g(g_0) \\ &= \frac{g_0}{N}\sqrt{-t\log_e(2\pi t g_0^2)} = (N\sqrt{2e\pi})^{-1} \end{aligned} \tag{17}$$

$$P(g < g_0) = 1 - F_g(g_0) \tag{18}$$

Dividing (17) by (18) gives the ratio of the probabilities of the two modes:

$$\frac{F_g(g_0)}{1-F_g(g_0)} = \underset{N\to\infty}{Limit} \frac{1}{N\sqrt{2e\pi}-1} << 1 \tag{19}$$

□

2.4 Scale life of the GMSS of a discontinuity

Theorem 5. The Scale-Life (SL) of a discontinuity (with a magnitude A), i.e the interval of scales ($t \in (0, SL)$) within which the discontinuity can be statistically identified by the unbalanced bimodality of the PDF of the GMSS of a discontinuity is given by:

$$SL = \frac{A^2}{2\pi\epsilon^2} \quad where \quad \epsilon = \text{Upper Bound of error} \tag{20}$$

Proof. From Theorem 1 for a discontinuity with a magnitude A, the GMSS will be given by:

$$L'(x;t) = \frac{Ae^{-\frac{x^2}{2t}}}{\sqrt{2\pi t}} \tag{21}$$

In a manner similar to proof of Theorem 2, it can be shown that the PDF ($f_g(g)$) of the GMSS (21), will be defined in the interval $g \in (0, A/\sqrt{2\pi t})$ with the second mode existing at $(A/\sqrt{2\pi t})$. For this mode to be identifiable as a separate mode it should be greater than or equal to (ϵ) i.e.

$$\frac{A}{\sqrt{2\pi t}} \geq \epsilon \Rightarrow t \leq \frac{A^2}{2\pi\epsilon^2} \tag{22}$$

□

The concept of an infinitesimal existence of a discontinuity in Scale-Space/Heat Equation is acknowledged by research community (Gonzalez-Velasco, 1995; Lindeberg, 1994; Widder, 1975), but seldom defined. Theorem 5 provides one (amongst plausibly many) rigorous definition of the life of a discontinuity, derived from (and therefore limited to) the statistics of the GMSS of a discontinuity.

Implication of (ϵ): Any discrete application of the theoretical results would invoke the upper bound of error(ϵ), and therefore needs to be understood in the context of discretization in general, and selection of histogram bin size in specific (in images/signals). The selection of bin size inadvertently defines (ϵ) and is dependent on:

1. Physical limitations of the sensor/hardware: E.g.a camera might be able to distinguish 8, 64 or 256 intensity levels depending on 3,6 or 8 bit representation. The upper bound of error (as measured with respect to absolute ambient intensity) for a 8 bit representation will be much lower than that of 3 bit representation.

2. Accuracy desired by the user: Even though the sensor is capable of higher precision (or lower error), an algorithm/user might require a lower precision, wherein the upper bound of error is artificially set at a higher value.

Hence the ability of algorithms to capture the unbalance and bimodality of the PDF within the Scale-Life will depend on the precision of the hardware as well as the bin size of the histogram.

2.5 Comments

The theoretical results of this section can be perceived to be at slight variance with the assumptions and models of a discontinuity in conventional scale-space, and the reasons for this variance will be discussed in this subsection. The widely accepted norm of *ignoring a discontinuity in Scale-Space and analyzing the underlying signal/image as if it were continuous*, can be attributed to the following factors:

1. *Requirement of Scale-Space framework*, to comply with the principles of homogeneity and isotropy, necessitates the framework to remain uncommitted to a gaussian scale. Consequently modeling a discontinuity as done in heat equation, would result in violation of the fundamental requirements of Scale-Space.
2. *Inadequate Information:* Most of the problems of Computer Vision, are related to identifying the presence/absence of a discontinuity followed by a contextual analysis of the discontinuity. In the absence of this basic information about the presence of a discontinuity, much less its properties like the magnitude and location of the discontinuity, it is difficult to model the transient presence of a discontinuity in Scale-Space.
3. *Absence of appropriate model:* Even if the location and magnitude of the discontinuity were available, a model to represent the discontinuity is difficult to prepare, because it leads to a lot of unanswered questions like how long does the discontinuity last? and, how to model the transfer from a discontinuous state to a continuous state?
4. *Mathematical simplification:* Theoretically a discontinuity disappears at an infinitesimal scale, therefore by ignoring this infinitesimal scale, a continuous model of a discontinuity can be mathematically justified.

The text (Theorems 1, 2 and 5) so far, is not meant to contradict or discredit existing conventions of Scale-Space , but to present a mathematically valid alternate representation of the Scale-Space. As an illustration of alternate (to Scale-Space) representations of a discontinuity, consider the heat equation (Gonzalez-Velasco, 1995; Widder, 1975). In heat equation a discontinuity may be explicitly modeled in following mathematically valid conventions:

1. As a Neumann Boundary Condition which specifies the rate of temperature (equivalent to intensity) change at the boundary.
2. As a heat source in space delimited by boundaries.

These alternate models adopted by a broader theoretical framework of heat equations, illustrate the need to represent a discontinuity in forms other than the one adopted in conventional Scale-Space theory. The PDF of the GMSS of a discontinuity (Theorems 1, 2 and 5)is an alternate representation of a discontinuity, which is unaltered in the Scale-Life (Theorem 5) including the zeroth scale. The unbalanced bimodality of the PDF can be applied homogeneously across the scales for the Scale-Life of a discontinuity, without the ambiguity of modeling or ignoring a transition from a discontinuous state to a continuous state.

This section provides a mathematical expression for the the PDF of a Gaussian Function, with a universal applicability for disciplines employing Gaussian Functions e.g. inverse problems of heat equation, chemical diffusion and Scale-Space Theory. The unbalanced bimodality of the PDF of a Gaussian Function facilitates interpretation of the second mode of the PDF as a statistical outlier. Consequently any problem of a discontinuity detection can be reformulated as a statistical problem of outlier detection. The sections hereon can be viewed as one application of the general results of this section, wherein a statistical parameter (OT) sensitive to outlier data, is used to detect a discontinuity in images.

3. OT: Unbalanced histograms

In this section a general review of OT will be presented and an expression of OT for unbalanced bimodal PDF will be developed for 1-Dimensional function, with a view to accommodate the GMSS of a discontinuity. OT is statistically generated from a normalized

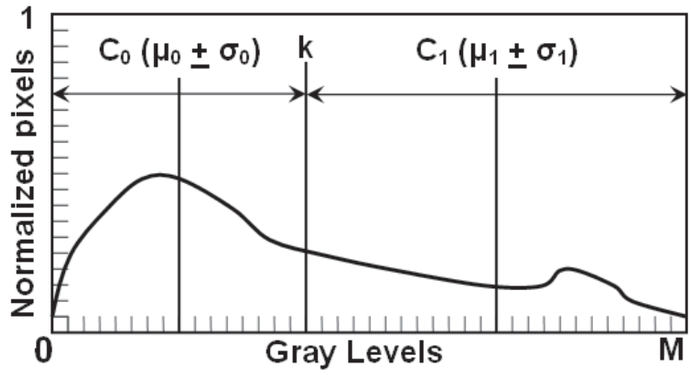

Fig. 4. Schema: Otsu's Threshold (which maximizes the Between Class Variance) in a histogram.

histogram with M bins corresponding to M gray levels in an image (Figure 4). Each bin represents the percentage of the pixels in the image with corresponding gray level. This normalized histogram is bifurcated into two classes C_0 and C_1 at a hypothetical threshold (k). The hypothetical threshold (k), Means (μ_0, μ_1) and Standard Deviations (σ_0, σ_1) of two classes are shown in Fig 4. The maximum of Between Class Variance (BCV) determines the appropriate threshold (OT). BCV ν_B is defined by 23:

$$\nu_B = \omega_0(\mu_0 - \mu_T)^2 + \omega_1(\mu_1 - \mu_T)^2 \quad \textit{where} \tag{23}$$

$$\omega_0 = \sum_{i=0}^{k} p_i, \quad \omega_1 = \sum_{i=k+1}^{M} p_i \tag{24}$$

0^{th} *order Cumulative Moment for* C_0 *and* C_1

$$\mu_T = \sum_{i=0}^{M} ip_i, \gamma_k = \sum_{i=0}^{k} ip_i \tag{25}$$

1^{st} *order Cumulative Moment up to M and k*

$$\mu_0 = \frac{\gamma_k}{\mu_T}, \mu_1 = \frac{\mu_T - \gamma_k}{\mu_T} \tag{26}$$
$$\textit{Mean Gray Levels for } C_0 \textit{ and } C_1 \textit{ respectively}$$

$$p_i = \frac{n_i}{N_T} : \textit{Normalized probability at gray level i} \tag{27}$$
$$n_i, N_T : \textit{No of pixels at gray level i, Total pixels}$$

Theorem 6. OT (which maximizes BCV) is obtained at gray level (k*) defined by:

$$k^* = \frac{\mu_0 + \mu_1}{2} \tag{28}$$

Proof. Differentiate ν_B (23) with respect to gray levels (k) and equate to zero. For details see Lin (2003). □

The proof (Lin, 2003) is for histograms, but the results can easily be generalized to continuous PDFs. One solution of Theorem 6 is when the OT exists at the function/image mean.

Corollary 1. The maximum of BCV is obtained at the image mean (μ_T) if and only if the probabilities of the two classes are equal:

$$k^* = \mu_T \quad \Longleftrightarrow \quad \omega_0 = \omega_1 = 0.5 \tag{29}$$

Proof (If). Substituting $\omega_0 = \omega_1 = 0.5$ in μ_T (25):

$$\begin{aligned} &\mu_T = \mu_0\omega_0 + \mu_1\omega_1 \\ &\mu_T = 0.5\mu_0 + 0.5\mu_1 \qquad \square \\ &\mu_T = k^* \qquad \textit{from (28)} \end{aligned}$$

Proof (Only if). Equating μ_T (25) to k^* (28).

$$\begin{aligned} &\frac{\mu_0 + \mu_1}{2} = \mu_0\omega_0 + \mu_1\omega_1 \\ &\textit{substituting } \omega_0 = 1 - \omega_1 \textit{ from (24)} \qquad \square \\ &\omega_0 = \omega_1 = 0.5 \end{aligned}$$

Corollary 1 allows analysis of the OT in terms of the function/image mean, without constructing a PDF/histogram. Some of the plausible distributions mentioned by Lin (2003) where Corollary 1 is applicable are *unimodal, perfectly balanced bimodal and unbalanced bimodal*. Corollary 1 can be tailored to a PDF containing two linearly separable classes with unbalanced probabilities (Figure 5). This is done with a view to develop an expression for OT, applicable to the PDF of a Gaussian function.

Let a random variable $\mathbf{Q} = \{q \in (0, q_{end})\}$ with PDF $f_q(q)$ be composed of two populations (NC, IC) which are linearly separable at $(q = \psi)$ having distributions $f_{nc}(q)$ and $f_{ic}(q)$ respectively, such that

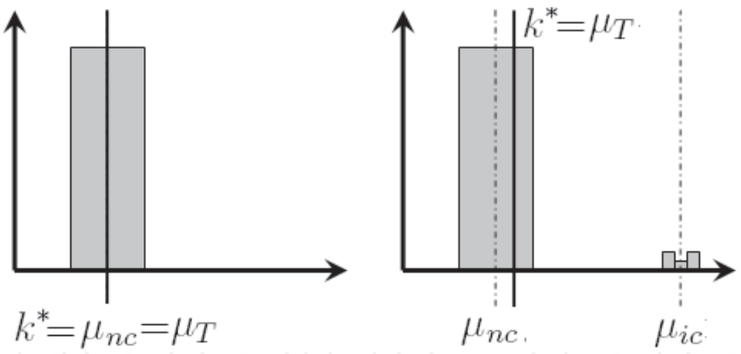

Fig. 5. OT Schema: (Left) Symmetric PDF and (Right) Unbalanced dual-class PDF (larger class is Symmetric about its mean)

$$f_q(q) = \left\{ \begin{array}{ll} m_{nc} f_{nc}(q) & if \quad q < \psi \\ m_{ic} f_{ic}(q) & else \end{array} \right\} \quad where$$

a.	$\psi \in (0, q_{end})$ Point of linear separation of two classes
b.	$m_{ic} = \frac{q_{end} - \psi}{q_{end}}, m_{nc} = \frac{\psi}{q_{end}}$ Probabilities of the two classes
c.	μ_{ic}, μ_{nc} Averages of the two classes
d.	$m_{ic} << m_{nc}$ PDF is Unbalanced
e.	$\mu_{ic} m_{ic} + \mu_{nc} m_{nc} = \mu_T$ Average value of the variable q
f.	$\mu_{ic} > \mu_{nc}$ Order of classes
g.	$f_{nc}(\mu_{nc} - q) = f_{nc}(\mu_{nc} + q)$ $\forall (q < \mu_{nc}) : f_{nc}(q) \neq 0$ $f_{nc}(q)$ is symmetric about μ_{nc}

(30)

Equation (30) presents a PDF which is a super-set of the PDF of a Gaussian function with following salient features:

1. It is unbalanced.
2. It is not strictly Bimodal, but accommodates bimodal PDFs.
3. Has an additional requirement of symmetry of the first mode about its mean, which is satisfied by a Gaussian function's PDF under limiting conditions (proof follows in Corollary 2).

Theorem 7. For a PDF of the kind (30), the OT is given by:

$$k^* = \mu_{nc} + m_{ic}(\mu_{ic} - \mu_{nc})$$

Proof. First consider that the PDF consists of *only NC*, i.e:

$$(f_q(q) = f_{nc}) \iff (\psi = q_{end}, \mu_T = \mu_{nc} \; and \; m_{ic} = 0)$$

The probability of two halves of the PDF separated at a mean value ($k^* = \mu_T$) is ($\omega_0 = \omega_1 = 0.5$) (Figure 5 Left). Therefore from Corollary 1:

$$k^* = \mu_{nc} = \mu_T \tag{31}$$

If class (ic) with a very small probability $(m_{ic} << m_{nc})$ is added to this distribution (Figure 5 Right), then the OT and the PDF mean (μ_T) will change slightly, because for a very small change in μ_T, applicability of Corollary 1 will persist (Lin, 2003):

$$\begin{aligned} k^* = \mu_T &= m_{nc}\mu_{nc} + m_{ic}\mu_{ic} \\ &= \mu_{nc} + m_{ic}(\mu_{ic} - \mu_{nc}) \end{aligned} \tag{32}$$

□

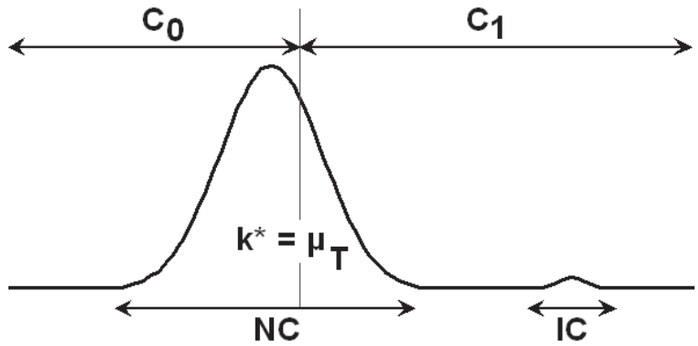

Fig. 6. Schematic illustration of two sets of classes :(C_0 and C_1) and (NC, IC) in an unbalanced PDF.

Schematic illustration of two sets of classes as discussed so far: (C_0 and C_1) and (NC, IC) in an unbalanced PDF is shown in Fig 6. The First set (IC and NC), appears as two separate distributions in the PDF. The second set of classes (C_0 and C_1) exists due to the hypothetical bifurcation of the PDF at OT. Equation (30) imposes less rigorous conditions for application of Theorem 7 for unbalanced PDFs as compared to (Lin, 2003). The PDF need not be strictly bimodal as long as it is unbalanced and the larger class (NC) is symmetric about its mean. In the next section, Theorem 7, will be adapted specifically for the PDF of a Gaussian function. The unique inverse J Shape (Figure 3) of the PDF of the Gaussian function implies that the PDF is concentrated around a value of zero. Thus by providing a rigorous definition of zero ϵ and its associated spatial domain ($\delta(t)$), following simplifications of Theorem 7 can be achieved:

1. Definition of point ψ in (30) and consequently linear separation of the PDF of the Gaussian Function into IC and NC.
2. Expressions for average values and the probabilities of the two classes IC and NC.
3. Proof of PDF's i.e. unbalance $m_{ic} << m_{nc}$.
4. Elimination of need to prove symmetry of bigger class (NC). Proof is provided in the next section.

4. OT for a Gaussian function

Formal definition of zero (ϵ) and the corresponding spatial domain $\delta(t)$, is obtained from Cauchy's Epsilon-Delta $(\epsilon, \delta(t))$ definition (Felscher, 2000) as applied to limit of $G(x;t)$ when $x \to \infty$.

Theorem 8. If $(\epsilon, \delta(t) \in \Re^+)$ represent the real and positive upper bounds of error, for the Gaussian function $(G(x;t))$ and the associated spatial variable (x) respectively, where ϵ can be made infinitesimally small and $\delta(t)$ depends continuously on ϵ and scale (t), then the limit of the Gaussian function when $x \to \infty$ is given by:

$$\lim_{x \to \infty} G(x;t) = 0 \tag{33}$$

Alternatively for a given ϵ and a scale (t) there exists a $\delta(t)$, such that for all x belonging to the interval $(\|\delta(t)\|, \|\infty\|]$, the Gaussian function takes a value less than ϵ:

$$\exists \delta(t) : \forall x \in (\|\infty\| > \|x\| > \|\delta(t)\|) \Rightarrow \|G(x;t)\| < \epsilon \tag{34}$$

Proof. It is trivial to show from the definition of G(x;t) (1), that for a given ϵ following value of $\delta(t)$ provides the interval $(\|\delta(t)\|, \|\infty\|]$ for which $(G(x;t) < \epsilon)$:

$$\delta(t) = \sqrt{-t \log_e (2\pi t \epsilon^2)} \tag{35}$$

□

Magnitude (A) instead of unity, will change (35) to:

$$\delta(t) = \sqrt{-t \log_e (\frac{2\pi t \epsilon^2}{A^2})} \tag{36}$$

Graph of $\delta(t)$ from (36) at various ratios of (ϵ / A) for a Step Discontinuity is shown in Figure 7.

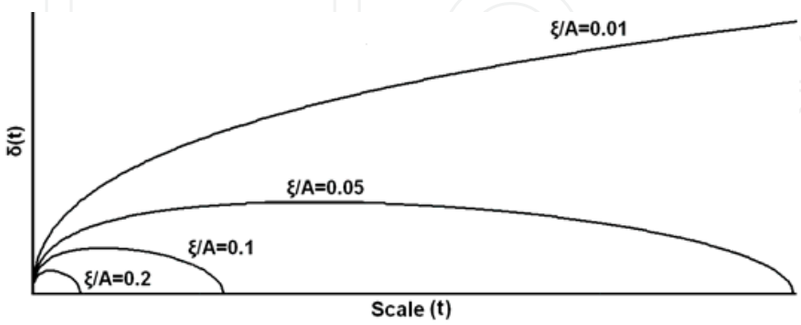

Fig. 7. Graph of $\delta(t)$ from (36) at various ratios of (ϵ / A) for the GMSS of a Discontinuity.

The graphs show that a maximum exists in each plot. At this point IC and NC can be defined in the context of the Gaussian Function with the help of ϵ.

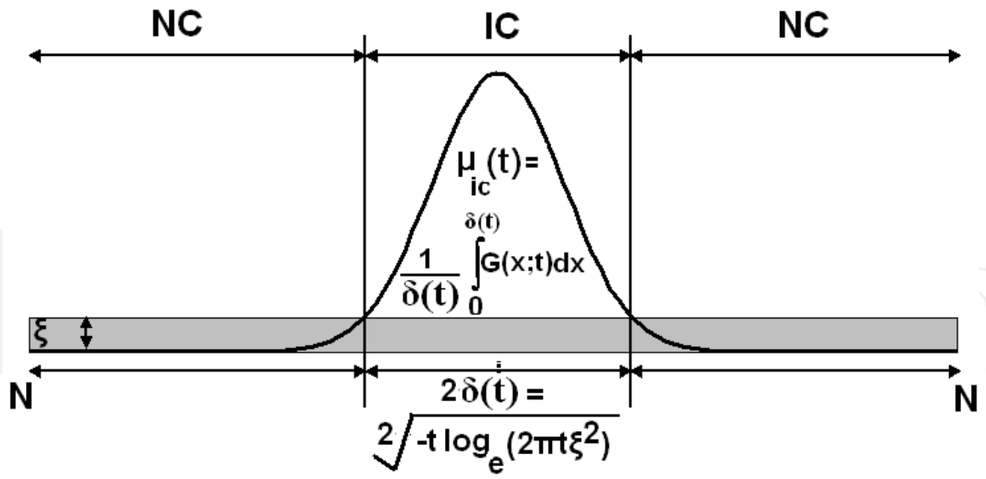

Fig. 8. GMSS of a Unit step (Gaussian) function along with various parameters of IC and NC.

4.1 Definition and statistics: IC and NC

Definition 1. Interface Class (IC) at scale (t) is defined as the spatial domain of the Gaussian Function where the value of the Gaussian Function is greater than the upper bound of error (ϵ).

$$\begin{aligned} IC(t) &= \{x \in N : G(x;t) > \epsilon\} \Rightarrow \\ IC(t) &= \{x \in N : x < \delta(t)\} \end{aligned} \tag{37}$$

Definition 2. Non-interface Class (NC) at scale (t) is defined as the spatial domain of the Gaussian Function where the value of the Gaussian Function is lesser than or equal to the upper bound of error (ϵ).

$$\begin{aligned} NC(t) &= \{x \in N : G(x;t) \leq \epsilon\} \Rightarrow \\ NC(t) &= \{x \in N : x \geq \delta(t)\} \end{aligned} \tag{38}$$

Figure 8 depicts the two classes IC and NC in the context of a Gaussian Function. Based on the above definitions the statistics of IC and NC can be determined.

Class	Statistic
NC	Mean: $\mu_{nc}(t) = 0$ Probability: $m_{nc}(t) = \dfrac{N - \delta(t)}{N}$
IC	Mean: $\mu_{ic}(t) = \dfrac{1}{\delta(t)} \displaystyle\int_0^{\delta(t)} G(x;t)dx$ Probability: $m_{ic}(t) = \dfrac{\delta(t)}{N}$

(39)

4.2 Applicability of theorem 7

Corollary 2. Bifurcating the Gaussian function $(G(x;t))$ or it's PDF $(f_g(g))$ at $(\psi = \epsilon)$, results in two classes IC and NC such that:

1. Two classes have an unbalanced probability.

$$P[g < \epsilon] >> P[g \geq \epsilon] \tag{40}$$

2. The larger class NC can be assumed to be symmetric about its mean μ_{nc}

Proof (Unbalance). Since $G(x;t)$ provides a one to one, monotone mapping from x to g and x is uniformly distributed over the interval $(0, N : N \to \infty)$, therefore the ratio of probability of NC to IC is given by:

$$\frac{P[g < \epsilon]}{P[g \geq \epsilon]} = \frac{P[x > \delta(t)]}{P[x \leq \delta(t)]} = \underset{N \to \infty}{Lt} \frac{N - \delta(t)}{\delta(t)} >> 1 \tag{41}$$

□

Proof (Assumption of Symmetry of bigger class). The domain $g < \epsilon$ of the NC in the PDF is infinitesimally small, lesser than the upper bound of error and consequently immeasurable. The PDF of (NC) can be computed by applying the limits $(g \to 0^+)$ to (5).

$$\underset{(g \to 0^+)}{Lim} f_g(g) = \underset{(g \to 0^+)}{Lim} \frac{t}{Ng\sqrt{-t\log_e(2\pi t g^2)}} = \frac{\sqrt{t}}{N} \underset{(g \to 0^+)}{Lim} \frac{1/g}{\sqrt{\log_e(2\pi t g^2)^{-1}}} \tag{42}$$

Equation (42) is of the form $(\frac{\infty}{\infty})$, therefore a simplification of (42) is possible by the application of *L'Hopital's Rule*, i.e. differentiating both the numerator and the denominator w.r.t (g).

$$\frac{\sqrt{t}}{N} \underset{(g \to 0^+)}{Lim} \frac{\frac{\mathrm{d}}{\mathrm{d}g}(\frac{1}{g})}{\frac{\mathrm{d}}{\mathrm{d}g}(\sqrt{\log_e(2\pi t g^2)^{-1}})} = \frac{\sqrt{t}}{N} \underset{(g \to 0^+)}{Lim} \frac{\sqrt{\log_e(2\pi t g^2)^{-1}}}{g} = \infty \tag{43}$$

Since the PDF $(f_g(g))$ has a value of infinity in an infinitesimal interval $(g < \epsilon)$, therefore the PDF in the interval $(g < \epsilon)$ can be approximated by a Dirac Delta. The Dirac Delta is the limiting case of the Symmetric Gaussian Function (with zero standard deviation), therefore assumption of symmetry of the PDF of the NC is justified. □

Corollary 2 implies that Theorem 7 is applicable for a Gaussian function where the IC and NC are separated at a Gaussian value $(G(x;t) = \epsilon)$ or at equivalent space coordinate $(x = \delta(t))$.

Theorem 9. The OT, for the GMSS of a step function is given by:

$$k^*(t) = \frac{1}{N} Erf[\delta(t)] \quad where \quad Erf[\delta(t)] = \frac{1}{\sqrt{\pi}} \int_0^{\delta(t)} e^{-p^2} \mathrm{d}p \tag{44}$$

Proof. Replacing $(\mu_{nc}(t) = 0)$ from (39) in Theorem 7:

$$k^*(t) = m_{ic}(t)\mu_{ic}(t) \tag{45}$$

Substituting $\mu_{ic}(t)$ and $(m_{ic}(t))$ from (39) and $(G(x;t))$ from (1) into (45) and solving:

$$k^*(t) = \frac{\delta(t)}{N\delta(t)} \int_o^{\delta(t)} \frac{e^{-\frac{x^2}{2t}}}{\sqrt{2\pi t}} \mathrm{d}x = \frac{1}{N} Erf[\delta(t)]$$

□

Plots of OT and $\delta(t)$ from Theorem 9 at various ratios of (ϵ/A) are shown in Figure 9. Both the plots $(k^*(t), \delta(t))$ contain a maximum, which can also be verified by differentiating (44) and (36) w.r.t scale (t).

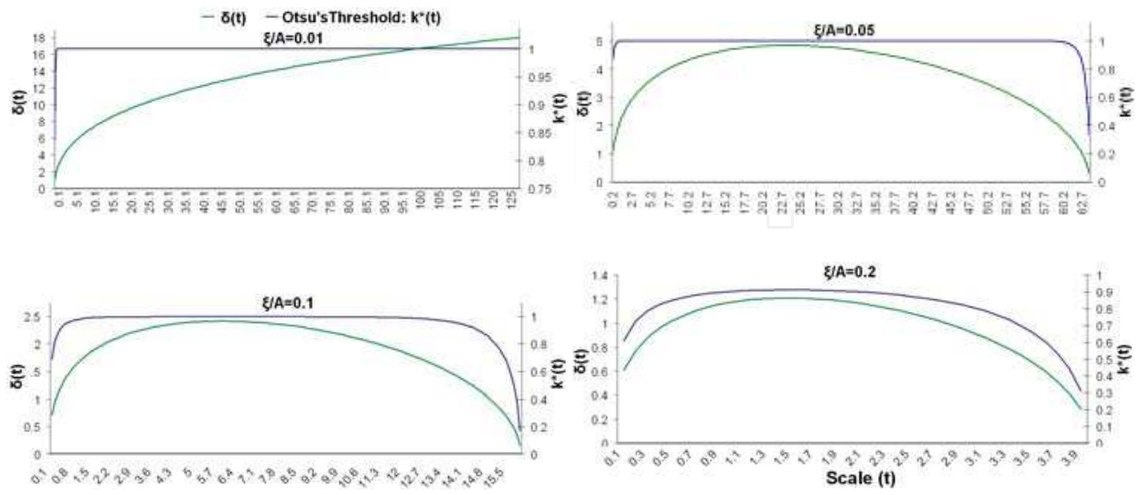

Fig. 9. Comparative Graphs of OT $[k*(t)]$ and $[\delta(t)]$ against Scale at various ratios of ϵ/A.

5. OT for continuous functions

Theorem 10. The OT for the GMSS of a continuous signal is monotonically decreasing i.e.

$$k^*(t) > k^*(t + \Delta t) \quad \forall \quad \Delta t > 0 \tag{46}$$

Proof. Due to the Central Limit Theorem, the PDF of the GMSS of a continuous function can be approximated by a normal (and consequently symmetric) distribution. Therefore from Corollary 1:

$$k^*(t) = \mu_T(t) \quad and \quad k^*(t + \Delta t) = \mu_T(t + \Delta t) \tag{47}$$

For continuous functions, the Maximum Principle is valid Gonzalez-Velasco (1995); Lindeberg (1994); Widder (1975). Due to the Maximum principle the GMSS of the continuous function (and its mean) will be monotonically decreasing with increase of scale (Babaud et al. (1986); Lindeberg (1994; 1998)), i.e. :

$$\mu_T(t) > \mu_T(t + \Delta t) \quad \forall \quad \Delta t > 0 \tag{48}$$

Combining (47) and (48)

$$k^*(t) > k^*(t + \Delta t) \quad \forall \quad \Delta t > 0 \qquad \square$$

Comparison of Theorem 9 with Theorem 10 reveals the contrasting patterns for OT when traced against scale:

1. Transient Increase: When a discontinuity exists.
2. Monotone Decrease: When a function is continuous.

6. Heuristic and algorithm for simultaneous scale, threshold and discontinuity detection

In this section, the theoretical results from non-discrete 1-Dimensional functions of the previous sections will be applied to the analysis of discrete 2-Dimensional images. Specifically the interface between the entities will be detected. The ideology underpinning this section is that the edges in images can be broadly classified as

a. *Boundary-Edges:* These edges correspond to interface between two entities of a 3D physical world, when projected onto the 2D image surface as a consequence of the process of image capture (e.g. an edge located at the interface of foreground-background). Since Boundary-Edges exist at the interface of heterogeneous surfaces or/and processes, the discrete gradient (Sobel) of Boundary-Edges is computed from dissimilar neighborhoods leading to a high intensity gradient and also spatial Scarcity, rendering Boundary-Edges similar to IC of the 1D functions.
b. *Non-Boundary-Edges:* In contrast, the Non-Boundary-Edges owe their discrete gradient computation to homogeneous neighborhood, resulting in low gradient and high spatial probability which is similar to NC of the 1D functions.

This apparent similarity, has empirical support from contemporary literature (Bhanu & Faugeras, 1982; Lin, 2003; Medina Carnicer & Madrid Cuevas , 2008; Rosin, 2001) wherein existence of unbalanced histograms for the derivative of images have been reported. The similarity of the histograms and the associated statistics (probability and mean) of IC and NC with Boundary-Edges and Non-Boundary edges respectively, allows for the development of a heuristic to extrapolate Theorem 9 and Theorem 10 for detection of Boundary-Edges. The problem of Boundary-Edges identification can be subdivided into:

1. Finding the optimum Scale
2. Finding the optimum Threshold at the Scale
3. Locating the interface, as the discontinuity travels in scale-space (Lindeberg, 1994).

To locate the Boundary-Edges, the following heuristic has been evolved which identifies both the scale and threshold appropriate to the interface using OT.

6.1 Heuristic

In the presence of an inflection in the plot of OT (calculated for the GMSS of an image) against incremental scale, it can be assumed that a discontinuity due to a foreground-background interface exists in the image. This discontinuity can be identified by thresholding the GMSS of the image at the scale and OT corresponding to the upper point of inflection in the plot of OT.

Justification: There are three aspects of the Heuristic i.e. presence of discontinuity, appropriate scale and appropriate threshold, which need to be justified individually:

1. *Presence of a discontinuity:* The presence of an inflection only in the presence of discontinuity has been shown via Theorem 9 and Theorem 10 for functions with and without a discontinuity respectively.

2. *Scale at upper point of inflection:* There is no universally agreed definition of appropriate scale; hence the justification of appropriate scale is qualitative rather than mathematical. The upper point of inflection is the scale appropriate for the discontinuity owing to following reasons:
   (a) Lower point of inflection wrongly classifies the pixels as belonging to IC (Figure 10). Hence for all scales lower than the lower point of inflection, false classification as IC is a strong possibility.
   (b) Experimentally and theoretically (most of the graphs of Figure 9), it has been observed that often from the lower to the upper point of inflection there is only small difference of scales. Hence attempting to locate the scale between the upper and lower points of inflection is mostly futile.
   (c) Scales greater than the scale at the upper point of inflection can give comparable results for the discontinuity identification as the scale at upper point of inflection, but at some scale greater than the upper point of inflection the IC will cease to exist. In the absence of a priori information of this scale where IC ceases to exist, using a scale greater than the one identified by the upper point of inflection, runs the risk of attempting to locate IC at a scale at which the IC does not exist. Therefore the upper point of inflection is the best scale for IC detection.
3. *OT at upper point of inflection as the threshold:*
   (a) OT at the upper point of inflection has been chosen as the threshold as it corresponds to the scale appropriate to the discontinuity.
   (b) Minimum False positives: The upper point of inflection represents the highest threshold intensity (utilizing OT in Scale-Space). Since the average value of the IC is greater than the rest of the image, therefore the highest threshold results in lowest false classification of the pixels as IC.

The application of the heuristics is demonstrated in Figure 10, wherein the Boundary-Edges have been located by thresholding at scale and OT corresponding to upper point of inflection[3]. Figure 10(a) depicts a synthetic image comprising of background only. A foreground is added to the texture of Figure 10(a) as shown in Figure 10(c) resulting in Figure 10(b). OT plotted against incremental scale for the GMSS of Figures 10(a) and 10(b) results in OT graphs shown in Figure 10(d), wherein the plot corresponding to the background only image has a monotonic decay in contrast to the image with a foreground which shows an inflection. Thresholding the image with the foreground (Figure 10(b)) at scale and OT corresponding to the upper point of inflection identifies the foreground-background interface.

6.2 Algorithm and results

Based on the Heuristic of the OT for discontinuity detection, a simple algorithm comprising of following steps can locate Boundary-Edges in images Walia & Jarvis (2009):

[3] The detection of the appropriate scale is not for a general discontinuity but conditional to the presence of a specific discontinuity. The discontinuity should be due to interface and therefore have an unbalanced histogram similar to the PDF in(30). The scale *cannot* be identified using the method presented here for discontinuities which are not due to interfaces.

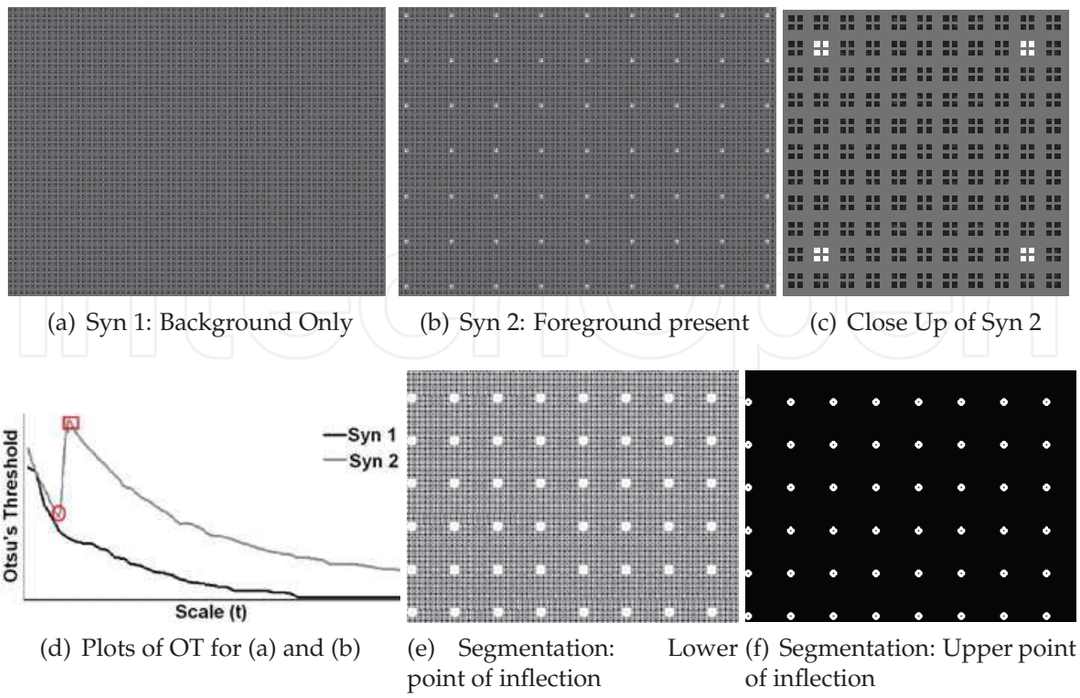

(a) Syn 1: Background Only (b) Syn 2: Foreground present (c) Close Up of Syn 2

(d) Plots of OT for (a) and (b) (e) Segmentation: Lower point of inflection (f) Segmentation: Upper point of inflection

Fig. 10. Illustration of Heuristic presented on Synthetic Images. (d) OT plots indicate a monotonic decay and an inflection in the absence and presence of a foreground (and consequent Boundary-Edge) respectively. (f) Upper point of inflection detects Boundary-Edges.

Algorithm 1: Simultaneous detection of scale, discontinuity and threshold in images

Compute the Sobel derivative of the input image;
while *Not end of Scale Range* **do**
    Convolve the Sobel derivative of the image, with a Gaussian Kernel of current scale;
    Compute histogram;
    Compute and record OT at current scale;
if *Increment of OT in plot against scale exists* **then**
    Identify the (scale, OT) pair at which the OT attains a maximum;
    Convolve the Sobel derivative of the input image with the scale identified;
    Threshold at the OT identified ;
else
    Output: No Discontinuity;

This chapter has discussed theoretical concepts behind the evolution of statistics of a discontinuity. It is difficult to provide a comprehensive comparison between the Algorithm 1 and other contemporary research because usage of *statistics* of Scale-Space representation of derivative of image/functions to identify discontinuity is a novel proposition. (Lindeberg,

1998) has done extensive research in the 1990's on automatic scale selection with applications in edge detection which can be used to compare the theory presented in this chapter. The differences with the approach of (Lindeberg, 1998) are :

1. Assumption of continuity of an edge in Scale-Space by Lindeberg. As a consequence occasionally (Lindeberg, 1994) relies on maximum principle, which does not hold when a discontinuity is present (Gonzalez-Velasco, 1995).
2. Lindeberg exploits individual properties (like edge strength, non-maxima suppression, blob volume, scale-normalized gradient magnitude, directional derivatives etc) of local spatial features (like blob, edge and ridge) in images, to rank and identify various features. The theory and algorithm of this article utilize, the collective statistics of image/signal to identify discontinuity and are therefore immune to errors (Walia & Jarvis, 2009) arising out of local spatial considerations. Both the approaches have contextual relevance.

OT is a well known method for segmenting images and therefore provides a good benchmark to compare the performance of the algorithm presented here. A comparison of the segmentations based on Algorithm 1 with OT is shown in Figure 12. Algorithm 1 had scale increments of 0.1, and histogram comprised of 255 bins. Figure 12 shows images having well defined IC. When OT is applied at zeroth scale, the probability $m_{ic}(0)$ of IC is very small, therefore the OT instead of segmenting IC from NC, segments the NC at approximately the mean of NC ($\mu_{nc}(0)$). In comparison tracing the OT in the GMSS of the images, results in identifying both the scale and threshold appropriate for identifying IC.

The images set used in Figure 12 originate from eclectic sources, without a ground truth so a simple measure was chosen to compare Algorithm 1 with Otsu's Algorithm (Otsu, 1979). The thresholded results of the two algorithms were stored as binary images (Figure 11(b) and Figure 11(c)). The difference in the number of positives (Figure 11(c)) between the Otsu's algorithm and Algorithm 1 expressed as a percentage of the total pixels in the image determined the improvement in the boundary classification. The average improvement in classification was computed for the dataset of images shown in Figure 12. Algorithm 1 had on an average 31.3% better classification of the foreground-background boundary owing to a reduction in false positives as compared to Otsu's Algorithm.

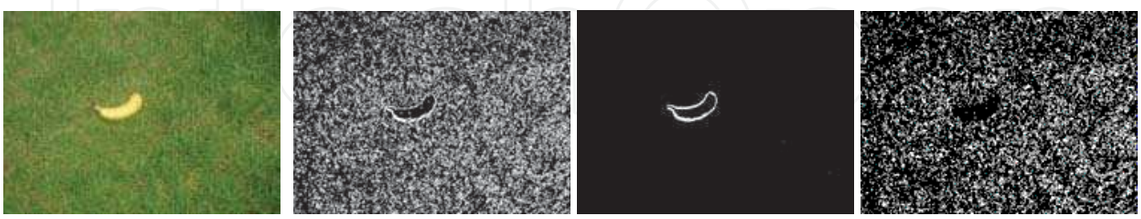

(a) Input (b) Otsu's Algorithm (c) Algorithm 1 (d) Eliminated False positives

Fig. 11. Algorithm comparison: Number of eliminated false positives (d=b-c) expressed as a percentage of the total pixels provides the improvement in boundary detection.

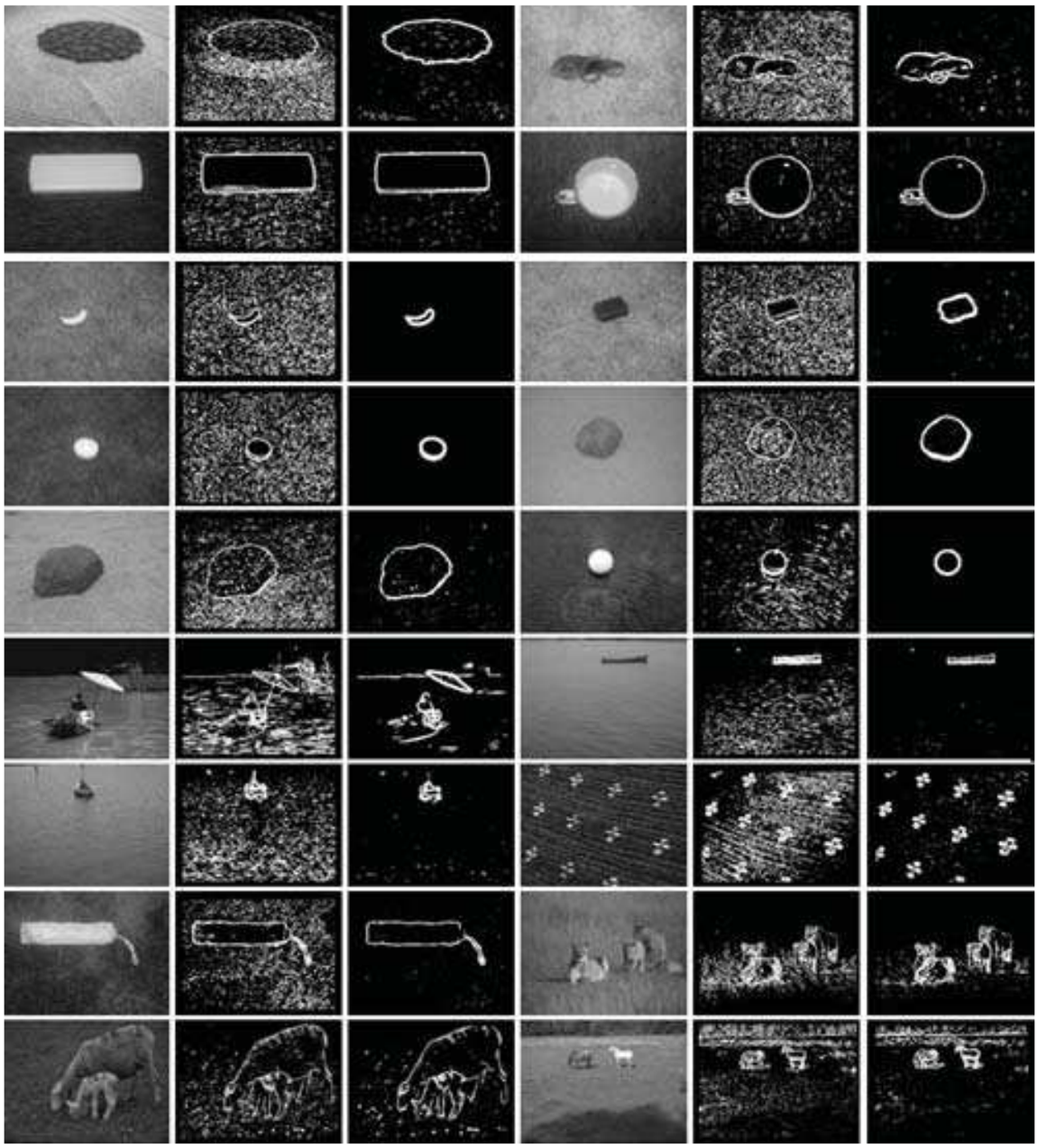

Fig. 12. Segmentation comparison . *Column 1 and 4:* Images with obvious boundaries.(some from Berkeley Dataset Martin et al. (2001)). *Column 2 and 5:*Thresholded by OT. *Column 3 and 6:* Thresholded at Scale and OT corresponding to inflection of OT.

7. Conclusion

Theoretical framework along with one application for characterization and identification of a discontinuity in Scale-Space framework for the derivative of image/function has been presented. This chapter shows that the PDF of the derivative of a discontinuity is unbalanced and bimodal in Scale-Space. By taking the derivative of functions/images, the discontinuities are formulated as outliers with higher average value and low probability. Since OT is a statistical parameter sensitive to the outliers (smaller mode in bimodal distribution) in a given data set, therefore it can detect and locate discontinuities. It is likely that many statistical parameters sensitive to outliers would exhibit similar response to discontinuities in scale-space.

8. References

Babaud, J., Witkin, A. P., Baudin, M. & Duda, R. O. (1986). Uniqueness of the gaussian kernel for scale-space filtering, *IEEE Trans. Pattern Anal. Mach. Intell.* 8(1): 26–33.

Bhanu, B. & Faugeras, O. D. (1982). Segmentation of images having unimodal distributions, *Pattern Analysis and Machine Intelligence, IEEE Transactions on* PAMI-4(4): 408 –419.

Duits, R., Felsberg, M., Florack, L. & Platel, B. (2003). α scale spaces on a bounded domain, *Lecture Notes in Computer Science* 2695: 494–510.

Eisenberger, I. (1964). Genesis of bimodal distributions, *Technometrics* 6(4): pp. 357–363.

Felscher, W. (2000). Bolzano, cauchy, epsilon, delta, *The American Mathematical Monthly* 107(9): 844–862.

Gonzalez-Velasco, E. (1995). *Fourier Analysis and Boundary Value Problems.*, Academic Press Limited.

Hubel, D. H. & Wiesel, T. N. (1987). Brain mechanisms of vision, *Nature* .

Kemperman, J. H. B. (1991). Mixtures with a limited number of modal intervals, *The Annals of Statistics* 19(4): pp. 2120–2144.

Khuri, A. I. (2004). Applications of dirac's delta function in statistics, *International Journal of Mathematical Education in Science and Technology* 35: 185–195.

Koenderink, J. (1984). The structure of images, *Biological Cybernetics* 50: 363–370. 10.1007/BF00336961.

Koenderink, J. J. & Doorn, A. J. V. (1992). Receptive field assembly pattern specificity, *Journal of Visual Communication and Image Representation* 3(1): 1 – 12.

Koenderink, J. J. & van Doorn, A. J. (1987). Representation of local geometry in the visual system, *Biol. Cybern.* 55(6): 367–375.

Lin, K. C. (2003). Fast image thresholding by finding the zero(s) of the first derivative of between-class variance, *Mach. Vision Appl.* 13(5-6): 254–262.

Lindeberg, T. (1994). *Scale Space Theory in Computer Vision.*, The Kluwer International Series in Engineering and Computer Science., Kluwer Academic Publishers, Netherlands.

Lindeberg, T. (1998). Feature detection with automatic scale selection, *International Journal of Computer Vision* 30: 79–116. 10.1023/A:1008045108935.

Martin, D., Fowlkes, C., Tal, D. & Malik, J. (2001). A database of human segmented natural images and its application to evaluating segmentation algorithms and measuring ecological statistics, *Proc. 8th Int'l Conf. Computer Vision*, Vol. 2, pp. 416–423.

Medina Carnicer, R. & Madrid Cuevas, F.J. (2008). Unimodal thresholding for edge detection, *Pattern Recognition* 41(7): 2337–2346.

Otsu, N. (1979). A threshold selection method from grey-level histograms, *SMC* 9(1): 62–66.

Rodriguez, R. (2006). A strategy for blood vessels segmentation based on the threshold which combines statistical and scale space filter: Application to the study of angiogenesis, *Computer Methods and Programs in Biomedicine* 82(1): 1–9.

Romeny, B. M. H. (1994). *Geometry-Driven Diffusion in Computer Vision.*, Kluwer Academic Publishers., Kluwer Academic Publishers, Netherlands.

Rosin, P. L. (2001). Unimodal thresholding, *Pattern Recognition* 34(11): 2083–2096.

Sakai, T. & Imiya, A. (2009). Unsupervised cluster discovery using statistics in scale space, *Engineering Applications of Artificial Intelligence* 22(1): 92 – 100.

Schilling, M. F., Watkins, A. E. & Watkins, W. (2002). Is human height bimodal?, *The American Statistician* 56(3): 223–229.

Walia, R. & Jarvis, R. (2009). Structure, scale-space and decay of otsu's threshold in images for foreground/background discrimination, *VISSAPP (2)*, pp. 120–128.

Widder, D. (1975). *The Heat Equation.*, Academic Press inc.

Witkin, A. P. (1983). Scale-space filtering, *IJCAI'83: Proceedings of the Eighth international joint conference on Artificial intelligence*, Morgan Kaufmann Publishers Inc., San Francisco, CA, USA, pp. 1019–1022.

Young, R. A. (1987). The gaussian derivative model for spatial vision: I. retinal mechanisms., *Spatial vision* 2(4): 273–293.

Zagal, J. C., Björkman, E., Lindeberg, T. & Roland, P. E. (2000). Significance determination for the scale-space primal sketch by comparison of statistics of scale-space blob volumes computed from pet signals vs. residual noise, *NeuroImage* 11(5, Supplement 1): S493.

Machine Vision - Applications and Systems

Edited by Dr. Fabio Solari

ISBN 978-953-51-0373-8

Hard cover, 272 pages

Publisher InTech

Published online 23, March, 2012

Published in print edition March, 2012

Vision plays a fundamental role for living beings by allowing them to interact with the environment in an effective and efficient way. The ultimate goal of Machine Vision is to endow artificial systems with adequate capabilities to cope with not a priori predetermined situations. To this end, we have to take into account the computing constraints of the hosting architectures and the specifications of the tasks to be accomplished, to continuously adapt and optimize the visual processing techniques. Nevertheless, by exploiting the low?cost computational power of off?the?shell computing devices, Machine Vision is not limited any more to industrial environments, where situations and tasks are simplified and very specific, but it is now pervasive to support system solutions of everyday life problems.

How to reference

In order to correctly reference this scholarly work, feel free to copy and paste the following:

Rahul Walia, David Suter and Raymond A. Jarvis (2012). Discontinuity Detection from Inflection of Otsu's Threshold in Derivative of Scale-Space, Machine Vision - Applications and Systems, Dr. Fabio Solari (Ed.), ISBN: 978-953-51-0373-8, InTech, Available from: http://www.intechopen.com/books/machine-vision-applications-and-systems/discontinuity-detection-from-inflection-of-otsu-s-threshold-in-the-derivative-of-scale-space

INTECH
open science | open minds

InTech Europe
University Campus STeP Ri
Slavka Krautzeka 83/A
51000 Rijeka, Croatia
Phone: +385 (51) 770 447
Fax: +385 (51) 686 166
www.intechopen.com

InTech China
Unit 405, Office Block, Hotel Equatorial Shanghai
No.65, Yan An Road (West), Shanghai, 200040, China
中国上海市延安西路65号上海国际贵都大饭店办公楼405单元
Phone: +86-21-62489820
Fax: +86-21-62489821

IntechOpen